Optimized Aperture for Estimating Depth from Projector's Defocus

Hiroshi Kawasaki , Yuki Horita , Hitoshi Masuyama , Satoshi Ono
Faculty of Engineering, Kagoshima University
{kawasaki,sc109063,sc109064,ono}@ibe.kagoshima-u.ac.jp

Makoto Kimura , Yasuo Takane
Samsung Yokohama Research Institute Co.,Ltd.
{m.kimura,y.takane}@samsung.com

Abstract

This paper proposes a method for designing a coded aperture, which is installed in a projector for active depth measurement. The aperture design is achieved by genetic algorithm. In this paper, a system for depth measurement using projector and camera system is introduced. The system involves a prototype projector with a coded aperture which is used to reconstruct a shape using Depth from Defocus (DfD) technique. Then, we propose a method to create a coded aperture to achieve the best performance on depth measurement. We also propose an efficient calibration technique on defocus parameters and a cost function for DfD to improve the accuracy and the robustness. Experimental results show that the proposed method can create an aperture pattern using simulation considering noise for fitness calculation. Evaluations are conducted to confirm that the proposed pattern is better than other patterns with our depth measurement algorithm.

1. Introduction

Recently, active 3D scanners are widely used for actual 3D model acquisition process. In particular, structured light systems [6, 1] have been intensively researched and commercialized due to their simplicity and accuracy. Those systems require the correspondences between projected pattern and observed pattern for triangulation calculation. For such correspondence estimation, many solutions were proposed, *e.g.*, sinusoidal patterns [18], Gray code [15], etc. To retrieve the correspondence accurately, the patterns should be captured sharply by the camera. Thus, both the camera and the pattern projector should be in focus on the target; it sets an implicit but severe condition for the system. Further, depth of field (DOF) of projector is usually shallower than that of camera because of a limitation on power of light source. Therefore, the DOF of projector limits the range of 3D measurement. One essential solution for the problem is to use special light source which emits straight beam without blur such as laser. However, making a dense 2D pattern with laser is not easy and using strong laser for consumer products is better avoided for safety reason.

In recent researches in the field of Computational Photography, Coded Aperture (CA) – non-circular shape aperture – is widely investigated [17, 8, 20, 19, 9]. CA allows many post-processes such as motion deblurring, all-focus image, Depth from Defocus (DfD), and so on. However few attentions have been paid on using CA on projector [5]. Recently, a DfD technique using a CA on a projector was proposed [7]. However, since they used CA for other purposes, captured patterns are severely distorted by a distance between a camera and a projector and its accuracy and robustness are limited.

In this paper, we propose a method to design an optimized coded aperture for DfD on projector using genetic algorithm(GA) [3]. In particular, a fitness value is calculated by physical simulation considering noise. We also propose a calibration technique on defocus parameters and a cost function for DfD to improve the result. Experimental results are conducted to show that the proposed system can measure depth with millimeter order and outperforms the other well-known aperture designs. Main contributions of this paper are as follows.

1. Optimized coded aperture for DfD on projector is designed by GA.
2. Defocus parameter calibration using small number of captured images is proposed.
3. Robust and accurate cost function for DfD using both intensity and spatial information is proposed.

2. Related work

In the field of Computer Vision, many active 3D measurement techniques have been researched and some of

them are commercially available [10, 11]. The methods based on triangulation using structured light have practical advantages in the cost efficiencies, because basically they only require simple hardware with non-specific devices. One drawback of the system is that the actual observed reflection often has ambiguity on obtaining correspondences. To resolve such ambiguity, many techniques have been proposed; *e.g.*, sinusoidal pattern [2, 18], Gray Code [15] or grid pattern [16, 14]. In this way, the past researches of structured light methods basically require sharp focus on the target object to resolve the correspondence between the projected pattern and the observed pattern; it limits the range for measurement. One of the solution for this problem is to use a focus-free pattern projection (*i.e.* laser beam) [11]. To avoid using lasers for safety reason, another solution using common light source is awaited.

The measurement of the depth from the defocused image is called "depth from defocus (DfD)" [13, 12] and mainly researched only on camera. Moreno-Noguer *et al*. [12] proposed DfD using pattern projector's defocus. They used a grid of dots, so that each observed dot's defocus can reflect its own depth information. In this method, any texture is not required in the scene. Since the final goal of the method was not 3D measurement and the depth data was used for image refocusing, the projection dot was sparse because they just need single depth for each segment. Instead, since our purpose is to measure the depth, dense pattern is required. In such case, patterns are inevitably overlapped each other when blur becomes large.

Recently, CA theory and techniques are researched in the field of Computational Photography [17, 8, 20, 19, 9]. In their research, they set specific aperture shape in the camera. Taking the advantage of the non-circular aperture, many special post-process (*e.g.* refocusing image, synthesis of all-focus image, DfD, etc) can be realized. In particular, Zhou *et al*. [20] and Masia *et al*. [9] created original CA design for defocus deblurring by means of GA, respectively. In contrast, there are very few researches about CA in projector. Grosse *et al*. proposed a data projection system including programmable CA [5].They assume situations of projecting to non-planar area, in which it is impossible to make the whole projected data focused by optics and applied pre-process to the projection data with consideration of CA and the target's depth map, so that the defocus amount in the out-of-focus area can be minimized to expand projector's physical DOF. Kawasaki *et al*. put a CA on projector to apply DfD on active 3D shape measurement [7]. Since they used the CA designed for other purposes and no precise calibration was conducted, accuracy and robustness are limited.

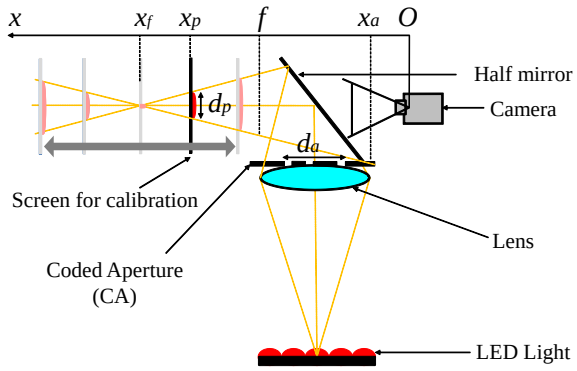

Figure 1. Optical configuration using a half mirror. x_p is a position of the target object, x_f is a focal position of the projector, f is a focal position of the camera, x_a is a position of the aperture, d_p is a diameter of the defocus blur, and d_a is a diameter of the aperture.

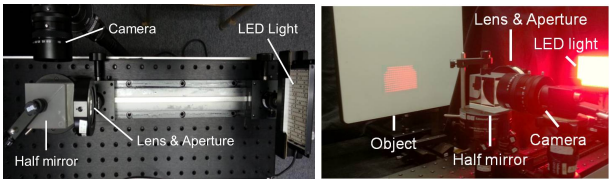

(a) top view (b) Capturing scene

Figure 2. Actual optical system using half-mirror and LED.

3. Shape from projector defocus

3.1. System configuration

The proposed system consists of lens, a projector, a camera and a CA. Since the proposed technique is based on DfD, it is ideal if the system has no baseline between a camera and a projector, so that the image can be captured without lens distortion and disparity, which makes a correspondence problem. Simple solution for the requirement is to use a half-mirror as shown in Fig.1. However, using half-mirror in this way causes several problems: 1) intensity of the projection in the scene is significantly reduced and a noise increases; 2) precise construction of the optics is required; 3) light bleeding effect from the original light source occurs. As for the first issue, we use independent LED as a pattern to keep strong light intensity. Also, a new cost function is developed for the shape reconstruction algorithm which is robust to noise (Sec.4.3). As for the second problem, we propose a calibration method which can precisely estimate the parameter of the system (Sec.4.2). The third problem is solved by simple image processing by capturing the biased image before measurement. Note that the resolution of LED array is low, however, it is not the limitation of the algorithm. An actual system is shown in Fig.2

3.2. Algorithm overview

With the proposed technique, depth is reconstructed by DfD technique using defocus blur of reflected light pattern

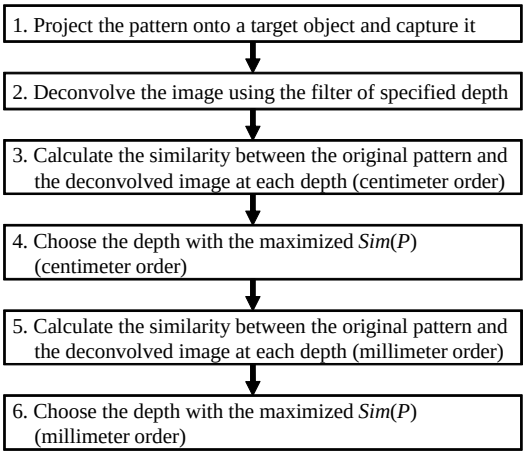

Figure 3. Reconstruction algorithm.

which is projected from the projector with CA. The defocus parameters of the projector are assumed to be calibrated. (details are described in Sec. 4.2).

Figure 3 shows the overview of the algorithm. First, patterns are projected onto the object and the scene is captured by a CCD camera. Since the captured image is biased by the original light source which directly comes through the half-mirror, the image must be unbiased by deducting the intensity which is previously captured by the camera without a target object. Second, we deconvolve the captured pattern from the unbiased image using a CA and a defocus parameter for specific depth. If the depth is same as the actual object depth, the deconvolved pattern should be same as the shape of the light source. Therefore, for the third step, we calculate the similarity between the two images by changing the depth for deconvolution. At the final step, the depth is retrieved by finding the best similarity. Since the method is based on an exhaustive search for every depth, a coarse to fine approach is applied; *i.e.*, we estimate the depth with large intervals and then same process is conducted with small intervals at the solution of coarse level.

One important advantage of our method is that the overlaps of the projected patterns do not affect the depth estimation. Another advantage is that since there is no baseline between the camera and the projector, there is no correspondence problem in our system, whereas which exists in [7].

4. Extended techniques for DfD on projector camera system

4.1. Optimized design of aperture by GA

In general, video projectors do not have an aperture, because it decreases the power of the light. Since projector's optics is similar to camera's one, if we put CA on the projector, several advantages of CA are also realized. For example, CA for improving the stereo algorithm for camera pair [19] could be applied to the projector and camera system [7]. However, such CA pattern is not guaranteed to work properly for the projector, because the CA pattern is optimized for the specific algorithm. Hence, we must create the CA pattern optimized for DfD on projector.

Designing an aperture is a combinatorial optimization problem whose search space size is $2^{N\times N}$, where a $N \times N$ binary pattern is utilized. In previous work for camera CA [20], N was set to 11, and the CA pattern was obtained by scaling up using optimization. the proposed method sets $N = 11$, but obtained a 13×13 pattern including surrounding closed cells.

Our GA optimization uses two-dimensional two-point crossover in which an offspring is generated by exchanging parents' strings in a rectangle region determined by randomly-chosen two points. Bit flip mutation, elite preservation and a simple generation alternation rule, in which parents are always replaced by offspring, are also used.

Fitness is calculated by a simulation as shown in Fig. 4. In the simulation, defocused images of several depths are synthesized from an aperture pattern, which is a phenotype of an individual string of GA. Deconvolution of every depth's PSF is applied to the defocused images. Then, fitness is calculated by the following equation:

$$F(x) = \min_{d} \left\{ Sim(\boldsymbol{P}_{d,d}) - \max_{d' \neq d} Sim(\boldsymbol{P}_{d,d'}) \right\}, \quad (1)$$

where $\vec{P}_{d1,d2}$ denotes a deconvolved image from a projected pattern of depth $d1$, using PSF at depth $d2$. $Sim()$ is a similarity function explained in Sec.4.3. Eq. (3) indicates that our fitness value is the worst margin of the appropriateness of depth estimation between correct and incorrect depths.

As mentioned, putting an aperture loses intensity of the projection. To help minimize the loss of the intensity, our GA has a constraint that more than a half of the aperture size must be opened.

4.2. Calibration of projector defocus

In our DfD algorithm, deconvolution is applied to the captured image using the defocus blur kernel of each depth; such kernels must be retrieved before shape measurement. Simple solution for the kernel acquisition is to measure the actual kernels for all the depths by observation [7]. In their method, since the kernel's shape does not drastically change with small depth change, the kernel shape are sampled with large intervals and represented by linear interpolation. If we can use an ideal point light source, the captured blur pattern can be considered as the PSF itself as shown in Fig.5. However, it is almost impossible to use an ideal point light source in reality, and thus, precise PSF cannot be measured. Another severe problem of this approach is that it completely depends on the observation. For CA design process using GA described in the previous section, blur simula-

Step 1:	Perform step 2 through 5 with changing a simulation distance as 250, 270, 300, 330, and 350(mm).
Step 2:	Make a simulated projection image that involves defocus blur by a convolution of a point light source with PSF whose size is obtained by the calibration.
Step 3:	Add noise to the projection image.
Step 4:	Deconvolve the projection image with PSF of correct depth, and calculate the similarity to the point light source.
step 5:	Deconvolve the projection image with PSFs of incorrect depths, and calculate the maximum similarity to the point light source.
step 6:	Let the fitness value be the worst margin of the appropriateness of depth estimation between correct and incorrect depths.

Figure 4. Pseudo code of depth estimation simulation for fitness calculation

(a)depth 250mm (b)depth 280mm (c)depth 300mm (d)depth 330mm (e)depth 350mm

Figure 5. Pattern of CA projected onto the screen

tion is obviously needed. Therefore, we need a parametric model to represent the blur kernel.

The shape of the blur kernel (*i.e.* PSF) is typically explained by four factors: aperture shape, defocus amount, aberration and noise. Among them, main variable of the defocus and the aberration is depth, whereas the aperture shape and the noise are constant. Further, shape deformation by defocus is more significant than aberration. In this paper, we only consider defocus to represent the blur kernel; *i.e.*, the deformation can be understood as a scaling of aperture shape with additive constant noise. Using the notation and the configuration in Fig.1, a scaling parameter can be calculated as the following equation:

$$S(x_p) = c\left(\frac{x_f}{x_p} - 1\right) \tag{2}$$

where c is a constant value calculated by $fd_a/(x_f - x_a)$. Therefore, we have only two unknown parameters in this model, and thus, minimum two images are required for the parameter estimation.

Fig.6 shows the procedure of the parameter estimation. At first, the blur pattern using CA is projected on a flat board, so that several images can be captured by changing the depth of the board. Since the captured pattern can be considered as a PSF itself, the size of the PSF could be directly measured from the image as the scaling parameter. However, it is difficult to accurately obtain PSF directly

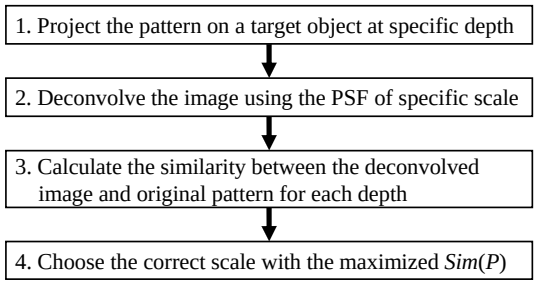

Figure 6. Calibration algorithm.

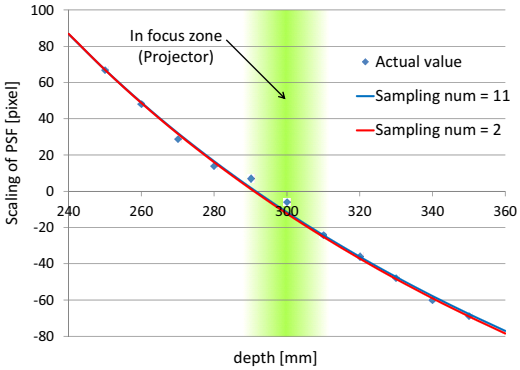

Figure 7. Scaling parameter estimation result.

from the captured images, because the images always have noise and other aberrations. Therefore, we take another way to estimate it as follows; we actually apply deconvolution to captured PSF, changing a scaling parameter to search the best parameter where deconvolved image is most similar to the original shape of light source. In this process, we use the same similarity function used in the shape reconstruction step described in Sec.4.3. In terms of deconvolution algorithm, we use Wiener deconvolution technique. Then, we use two pairs of the depth and the scaling value for defocus parameters estimation. An example of the estimation result is shown in Fig.7. We can confirm that the estimated curve well fit to the actual values.

4.3. Cost function for DfD

Similarity calculation is a key technique of our shape reconstruction algorithm. Unlike the common deblurring method which uses the perceptual quality metric for evaluation [9], we need to evaluates the similarity quantitatively. Since deconvolution is usually an unstable process, robust calculation is suitable. At the same time, to achieve high precision, sensitive function is preferable. Since these two requirements are somewhat contradictory, it is not easy to satisfy them with single metric.

In this paper, we use two metrics for solution. As for the first metric, we use a kurtosis of intensity distribution as following equation:

$$Sim(\boldsymbol{P}) = \sum_{i \in \boldsymbol{P}} \frac{(P_i - \bar{P})^4}{nV^2} - 3 \tag{3}$$

where $\boldsymbol{P} = \{P_1, P_2, ..., P_i, ...\}$ denotes a deconvolved image, P_i is the intensity of pixel i, n is the number of pixels in P, and V is a variance of the intensity histogram. As for the second metric, we use normalized cross-correlation (NCC) which is commonly used for image matching.

The kurtosis of the distribution is calculated from the histogram of the captured image. Since the deconvolved image with a correct kernel is getting closer to the original shape of the light source which looks like a single dot, the histogram of the image with correct kernel has a single peak near zero intensity (most pixels are dark). Therefore, the kurtosis can be used as a criterion to evaluate the deconvolved image; the higher kurtosis means the closer to the original shape. Although the kurtosis is robust in the meaning of global solution, it sometimes fails in local solution because it does not use spatial information. On the other hand, NCC compares not only the intensity distribution, but also spatial information. Therefore, similarity between two images can be calculated more accurately than the first metric. However, as known for stereo algorithms, the NCC is unstable if there are noise and outliers; it is actually the case for our method.

To compensate each drawback, we combine them with cascade approach; first we estimate the depth using maximum kurtosis of the histogram and if there are multiple solutions (*i.e.* if there are more than two peaks in the histogram), we apply NCC to select best one of them. Fig.8 shows two examples of captured images and Fig.9 shows the kurtosis of the histogram of deconvolved images. We can clearly see that Fig.8 (a) has single peak on kurtosis, whereas multiple peaks are observed for Fig.8 (b). However, such ambiguity is solved by NCC as shown in Fig.10.

5. Experiments

We conducted experiments to show the effectiveness of the method. The constructed system is shown in Fig2. We used an achromatic lens with 150mm focal length and 50mm diameter (Edmund Optics NT49-292-INK) with a half mirror. The camera was a Point Grey CCD camera with resolution 1280×960. We used an 18×12 array of 635nm LEDs as a dot pattern with light source, however, since a single lens usually has a strong aberrations near the peripheral region, we only used a center of the projected pattern for the experiments. Size of the CA was 35mm × 35mm and the distance between the lens and the light source was 300mm. We estimate the depth in 1mm order.

5.1. Evaluation of the optimized pattern with GA

To design the aperture pattern, we implemented a simulator for evaluation of CA appropriateness, and optimized aperture pattern for depth measurement. Parameters were configured as shown in Table 1.

(a) (b)

Figure 8. Two samples of defocused patterns of 280mm distance. Since LED shape and a distance are almost same, both patterns looks similar, however, the appearances of deconvolved images are different.

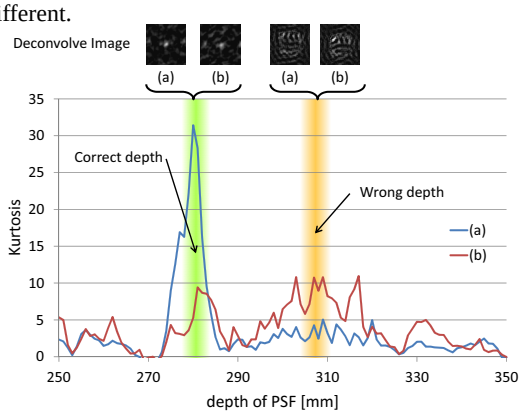

Figure 9. Kurtosis of the histogram.

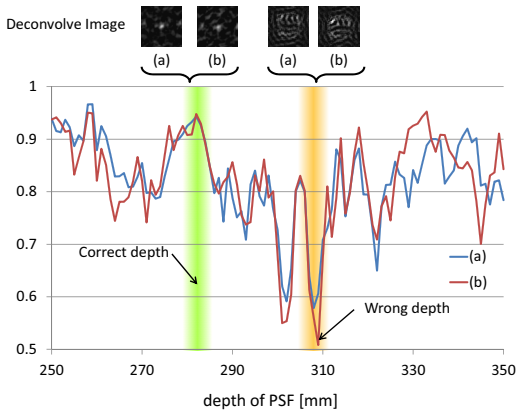

Figure 10. Normalized cross-correlation.

Table 1. Parameter configuration.

Population size	100
Generation limit	1,000
Number of elites	3
Crossover method	Two-point in 2D
Crossover rate	$\frac{100-3}{100}$
Mutation method	Bit flip mutation
Mutation rate	0.01
Resolution	11× 11
Noise level	$\sigma_1 = 0.00002\%$, $\sigma_2 = 0.001\%$
Deconvolution	Wiener filter
Simulation depth d	250, 270, 300, 330, 350 (mm)
d'	250, 270, 300, 330, 350, $d\pm5$ (mm)

Figs. 11 shows the example of fitness transitions in the evolution of GA. In this case, the fitness values were finally converged near 1,000 generations. Fig. 12 shows examples of the aperture patterns in the case with Gaussian noise

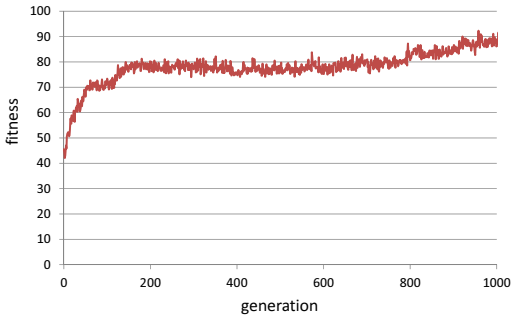

Figure 11. Fitness transitions in the case with noise (σ_1).

(a)initial pattern (b)optimized with σ_1 (c)optimized with σ_2

Figure 12. Optimized aperture by GA with difference noise level.

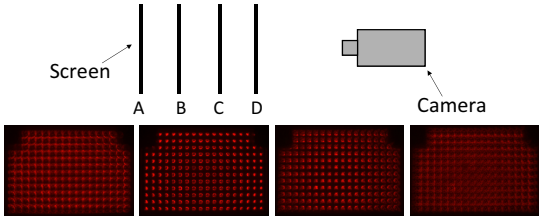

(a) (b) (c) (d)

Figure 13. Plane capture configuration.

whose average was set to 0. Several medium-large opened areas are seen in the outer area and small opened areas in the center area. In these patterns, detailed parts are decreased as noise increases. This is the same tendency as described in the previous work [20].

For evaluation, we estimated the depth of the flat board. Fig.13 shows the captured image. The light irradiated from the LED array is projected onto the board and the projected patterns are captured by the camera. Table 2 shows the captured patterns (left column) and deconvolved images by calibrated parameters of each depth. We can see that the deconvolved image of correct depth shows the sharpest pattern. The estimated depths are shown in Fig.14. In this experiment, largely overlapped areas of the projection patterns exist (*e.g.*, 87% for depth 250mm and 5% for 350mm). The conventional active 3D measurement methods can not work under such a condition. As shown in Fig.14, our proposed method reconstructed the depth correctly.

Then, we compared our aperture pattern with several well-known CAs as shown in Fig.15. Fig.16 shows the average and standard deviation of all the results. We can see that some apertures including ours performs more accurate with stronger blur; this is mainly because the patterns are asymmetry. Among the asymmetry apertures, our pattern is the best.

Table 2. Captured and deconvolved pattern in each distance.

Input \ Depth of filter	250mm	300mm	350mm
depth = 250mm, overlap = 87%	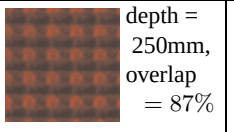		
depth = 300mm, overlap = none	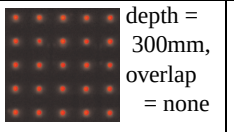		
depth = 350mm, overlap = 5%	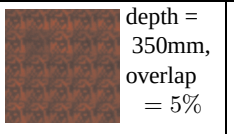		

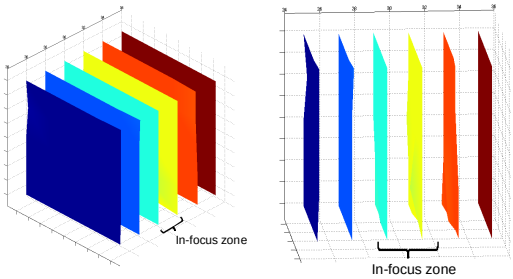

(a) Side view (b) Top view

Figure 14. Restoration of flat board results.

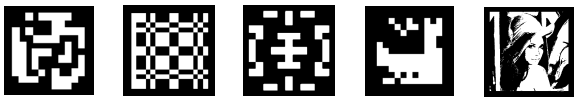

Zhou [20] MURA [4] Levin [8] Masia [9] Lenna

Figure 15. Coded Apertures used for comparison.

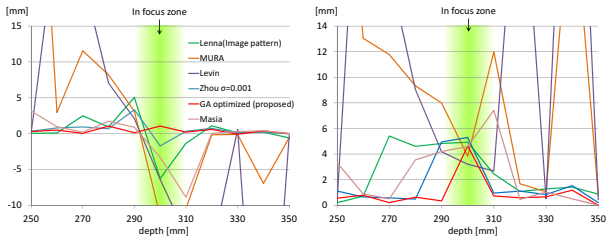

(a) Average error (b) Standard deviation

Figure 16. Average and standard deviation of the measured points in each depth. In-focus depth is 300mm.

5.2. Accuracies on textured object and occlusions

We evaluate our method with a textured object and objects with occlusions. For the textured object, we put checker patterns with green and white colors on the flat board as shown in Fig.17 (a). Projected patterns are strongly affected by textures as shown in Fig.17 (b). Fig.17 (c) shows the deconvolved image with the correct depth. In the image, the individual LED dot is successfully recovered. Fig.18

(a)Texture on the screen (b)Captured image (c)Deconvolve image

Figure 17. Captured and deblurred images of the textured screen.

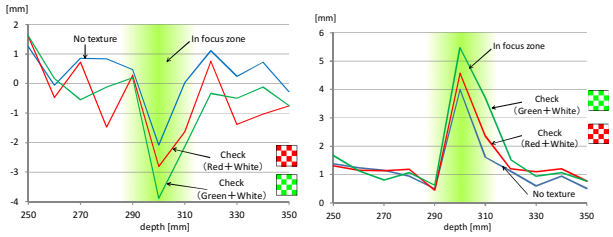

(a) Average error (b) Standard deviation

Figure 18. Average and standard deviation of the measured points on the textured screen in each depth.

(a) and (b) show the average error and standard deviation of the board with/without textures, respectively. The accuracy decreases if there is a texture on the board. However, all the results still keep enough accuracy even if the blurred patterns are overlapped and some of them are divided into several parts by color differences.

Next, occlusions are created by using two flat boards placing different depths as shown in Fig.19 (a). The left and the right boards are placed 270mm and 250mm from the lens, respectively. Fig.19 (b) shows the captured image and Fig.19 (c) shows the reconstructed shape. The shapes are correctly reconstructed, even though the patterns are separated by the border.

We also conducted the experiments where positions of the occluding boundaries are slightly changed as shown in Table.3 above. As the results shown in Table.3 bottom, the dominant depth is correctly reconstructed even if the patterns of different depths are overlapped to the target pattern. Such a stable reconstruction can be considered because of using a linear filter for deconvolution.

5.3. Shape reconstruction examples

Next, we estimated a depth of non-planar objects. First, we measured a box with textures as shown in Fig.20(a). The corner of the box was placed about 320mm from the lens and the farthest area was about 340mm, respectively. Fig.20(b) shows the captured image with reflected patterns and (c) shows the reconstruction results, in which the planes with $90\,\mathrm{deg}$ are successfully reconstructed. Next, we measured a cylinder with small bumps on the surface as shown in Fig.21 (a). Fig.21(b) shows the pattern of the CA projected onto it. The cylinder was placed nearest 320mm to furthest 340mm from the lens. Fig. 21 (c) shows the reconstruction results. The round shape is restored correctly even if the surface has strong bumps. Finally, our method is applied to the shape with curved surfaces with textures as shown in Fig.22 (a). Center of the object was placed 320mm apart from the lens. Fig.22(b) shows the reflected pattern and (c) shows the reconstruction results. In this case, the right top of the object was wrongly reconstructed. Such a problem is expected to be resolved by using dense pattern

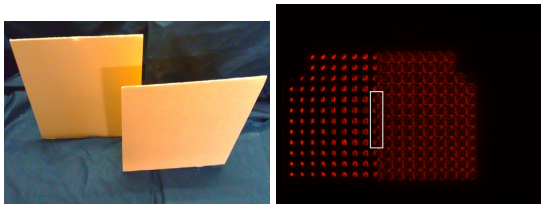

(a)Target object (b)Captured image

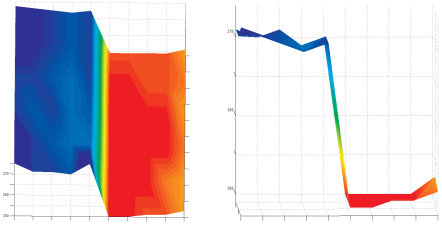

(c)Reconstructed result

Figure 19. Captured image and reconstructed result involving occlusion boundary.

Table 3. Captured image and estimation result involving occlusion boundary.

captured image	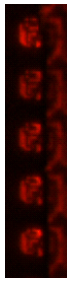	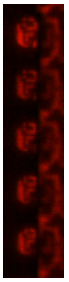	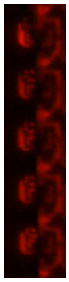	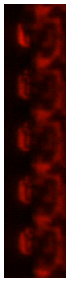
estimated depth[mm]	271	259	259	250
	272	270	258	250
	272	259	259	259
	272	271	259	259
	271	260	260	260

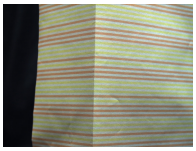
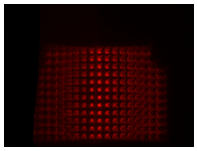

(a)Target object (b)Captured image

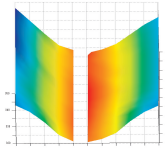
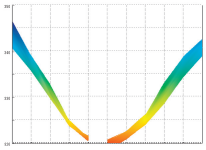

(c)Reconstructed result

Figure 20. Horizontal-striped box

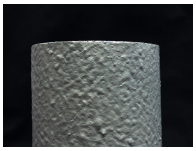
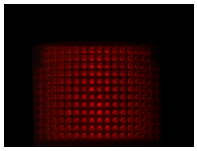

(a)Target object (b)Captured image

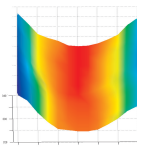
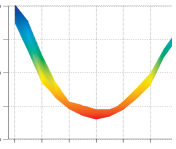

(c)Reconstructed result

Figure 21. Cylinder


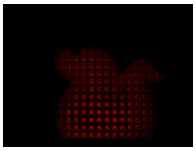

(a)Target object (b)Captured image

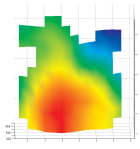
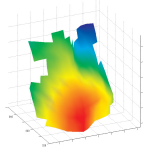

(c)Reconstructed result

Figure 22. Figure of snake

with better optics.

6. Conclusion

In this paper, we proposed an optimized coded aperture for 3D measurement system using projector defocus. Further, efficient calibration and cost functions were proposed to improve the accuracy and robustness. As the result, the 3D shapes are successfully measured by defocus of the projector and outperformed the other known coded apertures. In the future, increasing the resolution with better optics is important.

Acknowledgment

This work was supported in part by SCOPE No.101710002 and NEXT program No.LR030 in Japan.

References

[1] J. Batlle, E. M. Mouaddib, and J. Salvi. Recent progress in coded structured light as a technique to solve the correspondence problem: a survey. *Pattern Recognition*, 31(7):963–982, 1998.

[2] D. C. Ghiglia and M. D. Pritt. *Two-Dimensional Phase Unwrapping: Theory, Algorithms, And Software*. Wiley-interscience, 1998.

[3] D. E. Goldberg. *Genetic Algorithms in Search, Optimization, and Machine Learning*. Addison-Wesley, 1989.

[4] S. R. Gottesman and E. E. Fenimore. New family of binary arrays for coded aperture imaging. *Applied Optics*, 28(20):4344–4352, Oct 1989.

[5] M. Grosse, G. Wetzstein, A. Grundhöfer, and O. Bimber. Coded aperture projection. *ACM Trans. Graph.*, 29(3), 2010.

[6] S. Inokuchi, K. Sato, and F. Matsuda. Range imaging system for 3-D object recognition. In *ICPR*, pages 806–808, 1984.

[7] H. Kawasaki, Y. Horita, H. Morinaga, Y. Matugano, S. Ono, M. Kimura, and Y. Takane. Structured light with coded aperture for wide range 3d measurement. In *IEEE Conference on Image Processing (ICIP)*, 2012.

[8] A. Levin, R. Fergus, F. Durand, and W. T. Freeman. Image and depth from a conventional camera with a coded aperture. In *ACM SIGGRAPH 2007 papers*, SIGGRAPH '07, New York, NY, USA, 2007. ACM.

[9] B. Masia, L. Presa, A. Corrales, and D. Gutierrez. Perceptually optimized coded apertures for defocus deblurring. *Computer Graphics Forum*, 31(6):1867–1879, Sept. 2012.

[10] Mesa Imaging AG. SwissRanger SR-4000, 2011. http://www.swissranger .ch/index.php.

[11] Microsoft. Xbox 360 Kinect, 2010. http://www.xbox.com/en-US/kinect.

[12] F. Moreno-Noguer, P. N. Belhumeur, and S. K. Nayar. Active refocusing of images and videos. *ACM Trans. Graph.*, 26(3), July 2007.

[13] A. Pentland. A new sense for depth of field. *PAMI*, 9(4):423–430, 1987.

[14] R. Sagawa, H. Kawasaki, R. Furukawa, and S. Kiyota. Dense one-shot 3D reconstruction by detecting continuous regions with parallel line projection. In *ICCV*, pages 1911–1918, 2011.

[15] K. Sato and S. Inokuchi. Range-imaging system utilizing nematic liquid crystal mask. In *Proc. Int. Conf. on Computer Vision*, pages 657–661, 1987.

[16] A. O. Ulusoy, F. Calakli, and G. Taubin. One-shot scanning using de bruijn spaced grids. In *The 7th IEEE Conf. 3DIM*, pages 1786–1792, 2009.

[17] A. Veeraraghavan, R. Raskar, A. Agrawal, and A. M. andJ. Tumblin. Dappled photography: mask enhanced cameras for heterodyned light fields and coded aperture refocusing. *ACM Transactions on Graphics*, 2007.

[18] H. Zhao, W. Chen, and Y. Tan. Phase-unwrapping algorithm for the measurement of three-dimensional object shapes. *Applied Optics*, 33(20):4497–4500, 1994.

[19] C. Zhou, S. Lin, and S. K. Nayar. Coded Aperture Pairs for Depth from Defocus. In *IEEE International Conference on Computer Vision (ICCV)*, Oct 2009.

[20] C. Zhou and S. K. Nayar. What are Good Apertures for Defocus Deblurring? In *IEEE International Conference on Computational Photography*, Apr 2009.